Chapter 7
Atomic and Magnetic Force Studies of Co Thin Films and Nanoparticles: Understanding the Surface Correlation Using Fractal Studies

Indra Sulania, R. P. Yadav, and Ranjeet Kumar Karn

7.1   Introduction

Microscopy is a technique used for viewing those objects which cannot be seen with naked eyes. Zacharias Jansen and his father Hans were the persons who invented the first compound microscope in the late sixteenth century which enables us to look into the micrometer-scaled structures. Since then, many developments have happened that had made it possible for us to observe the structures in atomic scales. There are three well-known branches of microscopy: (i) *optical microscopy*, (ii) *electron microscopy*, and (iii) *scanning probe microscopy*. Optical microscopy (OM) is based upon the principles of reflection and refraction of light. In electron microscopy (EM), scattered electrons are collected to form the image of an object, whereas, in scanning probe microscopy (SPM), there is a physical interaction of a fine probe/tip with the surface of the sample which is capable of giving out the topography of a sample in three dimensions. Therefore, one can say it is the physical scanning of objects/samples with the help of a very small probe [1–3].

Scanning probe microscope is an instrument used for studying the surfaces at nanoscale regime. It forms images of surfaces using a physical probe that touches the sample's surface to scan it and collect data, typically obtained as a two-dimensional grid of data points and displayed as a computer image. The first SPM

I. Sulania (✉)
Inter University Accelerator Centre, New Delhi, India
e-mail: indra@iuac.res.in

R. P. Yadav
Department of Physics, Motilal Nehru National Institute of Technology Allahabad, Allahabad, India

R. K. Karn
University Department of Physics, Kolhan University, Chaibasa, India

instrument was developed in 1982 at the IBM Research Laboratory in Zurich by Gerd Binnig and Heinrich Rohrer and known as scanning tunneling microscope (STM) [4, 5]. It was the first technology to be recognized as having atomic resolution capability. It uses an electrical current between the microscope's scanning tip and the sample to image the surface of the sample. Unfortunately, the surface of the sample must be conductive or semiconductive, hence limiting the materials that can be studied using STMs [4]. These limitations drove the invention of the first atomic force microscope (AFM) [1, 3], and later magnetic force microscopy (MFM), electric field microscopy (EFM), conductive AFM, and AFM for liquid samples, which mainly find application in biological systems, etc., were developed together with STM in a single unit. Such instruments are called multimode, as they can be used to scan the samples in various modes, as per the requirement, using a proper interface between the software and hardware. AFM uses a very sharp tip to probe and map the morphology of a surface. However, AFM neither poses any requirement from the sample's side to be conductive, nor is it necessary to measure a current between the tip and sample to produce an image. AFM employs the tip or probe, at the end of a micro-fabricated cantilever with a low stiffness constant (spring constant) to measure the tip-sample forces as the tip presses (either continuously or intermittently) against the sample. Forces between the tip and the sample surface cause the cantilever to bend, or deflect, as the tip is scanned over the sample. The cantilever deflection is measured, and the measurements generate a map of surface topography. The details will be discussed in later sections.

In this chapter the basic principles of operation of an AFM will be presented, outlining the utmost common imaging modes and describing the attainment of force-distance measurements and techniques to calibrate cantilever spring constants. Further, we discuss the surface features such as shape and dimensions of the nano- and micron-sized particles, roughness of the surfaces, three-dimensional information of the surfaces and magnetic strength of the samples, biological sample scanning with the help of fluid cells to know the stiffness of the cell membranes, adhesion properties using the force-distance spectra, conducting properties with IV curves using conducting mode AFM, etc. Therefore, we can say that since the invention of AFM in 1986, it has become one of the most important tools for imaging the surfaces of samples at nanometric-scale resolution. Thus, it is considered to be a strong competitor to conventional methods, which are used to obtain the morphology of the samples and to investigate the structures, such as in electron microscopy, X-ray scattering, etc. In the beginning, atomic force microscopy (AFM) was applied almost exclusively to characterize the surfaces of non-biological materials. But we have cited few examples where the role of AFMs in imaging of biological samples is also highlighted. In the end, a few experimental examples are included to show the versatility of the techniques of AFM for the variety of samples. We will start our discussion briefly with scanning tunneling microscope. The detail about the STM is covered in another chapter of this book.

7.1.1 Scanning Tunneling Microscope

Scanning tunneling microscopy is a microscopy technique which helps us to investigate the electrically conducting surfaces down to the atomic scales, as it requires the tunneling of electrons from a conducting tip to the sample and vice versa depending upon the density of states of the electrons in the two. Here, quantum mechanical tunneling allows the particles to tunnel through a potential barrier which they could not do according to the classical laws of physics. Moreover, the probability of tunneling is exponentially dependent upon the distance of separation between the tip and surface, making the technique even more sensitive to investigate in atomistic levels.

7.1.1.1 Basic Working Principles of STM

The basic principle behind this instrument is the quantum mechanical tunneling of electrons when the tip and the samples are separated by a very small distance and a bias voltage is applied between them. The tunneling current flows across the small gap that separates the tip from the sample, a case that is forbidden in classical physics but that can be explained by the better approach of quantum mechanics: the electrons are "tunneling" across the gap. The tunneling current, "I," exhibits an exponentially decaying behavior with the separation between the tip and the sample. The relation is given by $I \propto U \exp(-kd)$, where k is a constant, U is the bias applied, and d is the tip-sample separation [2, 4, 5].

It is to be noted here that a very small change in the tip-sample separation induces large changes in the tunneling current. This behavior enables us to control the tip-sample separation very precisely. Furthermore, the tunneling current is mainly a contribution from the outermost atom of the tip, i.e., the atoms that are second nearest carry only a negligible amount of the current. Therefore, one can say that the sample surface is scanned with a single atom, which gives out the atomic resolution. As shown in the schematic in Fig. 7.1, the STM setup basically consists of a sharp conducting tip or probe, which is within angstrom distance from the sample, piezo scanners, and electronic control modules. Tip is attached with piezoelectric transducer. By applying a bias voltage between the tip and the sample, a "tunneling current" is generated. Tunneling current is converted into voltage by current amplifier which is then compared with reference value. The difference is amplified to derive z piezo. If absolute value of tunneling current is larger than the reference value, the voltage applied to z piezo tends to withdraw tip from sample surface and vice versa. The direction of current flow is determined by the polarity of the bias. If the sample is biased positive with respect to the tip, then electrons will flow from the tip to the surface and vice versa, as shown in Fig. 7.2.

Generally, the imaging of the surface topology can be carried out in two ways, either you keep the distance constant or you keep the current constant. This is described in details below:
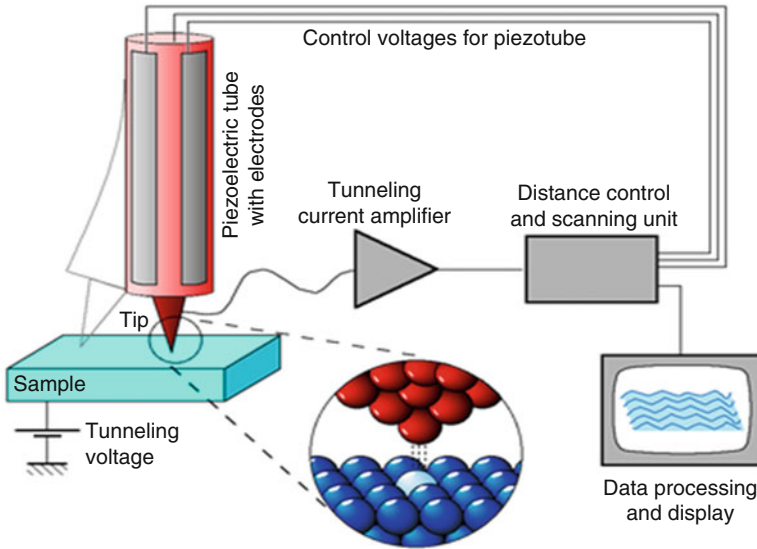
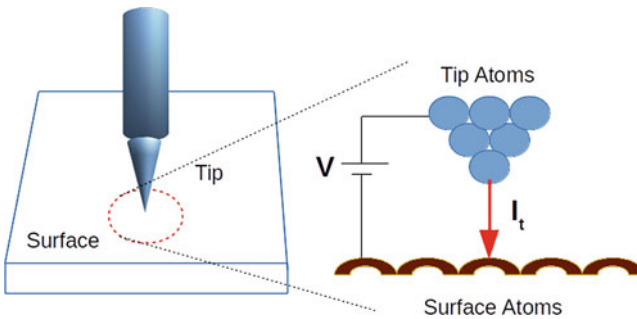**Fig. 7.1** Schematic of STM [Michael Schmid, TU Wien; adapted from the IAP/TU Wien STM Gallery]

Fig. 7.2 Sample bias and flow of tunneling current

7.1.1.2 Working Modes of STM

There are two main modes of working of STM – constant height mode and constant current mode.

Constant Height Mode

In constant height mode, the tunneling current is monitored as the tip is scanned parallel to the surface. If the tip is scanned at constant height above the surface (Fig. 7.3a), there is a periodic variation in the separation distance between the tip and
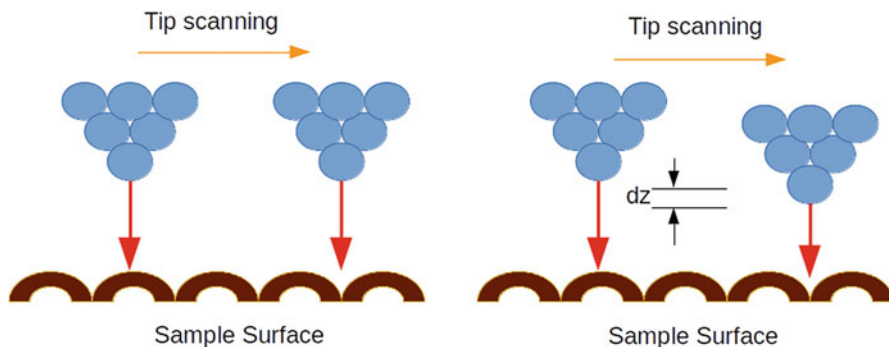
Fig. 7.3 Constant (**a**-left panel) height mode and (**b**-right panel) current mode

surface atoms. At one point the tip will be directly above a surface atom, and the tunneling current will be large, while at other points the tip will be above hollow sites and the tunneling current will be much smaller. Therefore, variation between tunneling current to tip's position gives the image of the surface.

Constant Current Mode

In constant current mode, the tunneling current is maintained constant as the tip is scanned across the surface. Generally, the normal way of imaging the surface is to maintain the constant tunneling current. This is done by adjusting the tip's height above the surface so that the tunneling current does not vary with the lateral tip position (Fig. 7.3b). Therefore, the tip will move slightly upward as it passes over a surface atom and, conversely, slightly in toward the surface as it passes over a hollow. The image is formed by plotting the tip height versus the tip position.

Limitation Although STM is capable of giving out the images in atomic scales, it could only be helpful for the conducting surfaces; this limitation led to the invention of atomic force microscopy (AFM) in 1986.

7.1.2 Atomic Force Microscopy

Atomic force microscope (AFM) is based on the sensing of the van der Waals interactions between the tip and the sample. AFM is used to investigate the samples by measuring forces between a sharp probe (<10 nm) and surface at very narrow distances (probe-sample separation) typical in the order of ∼0.2 to 10 nm. It was invented in 1986 by Binning et al.; since then, it has undergone many developments. The first AFMs were operated in contact mode (see Binning et al. [5]).

7.1.2.1 Basic Working Principles of AFM

In AFM, a probe is supported on a flexible cantilever analogous to tip attached to a spring as shown in Fig. 7.4. The force exerted by the tip onto the sample is given by Hooke's law. Therefore, by observing the deflection of the probe due to various forces acting between the tip and the sample (separated at a distance of 0.1–100 nm), the topography of the sample can be obtained in the form of two- or three-dimensional information [6–10].

These forces can be broadly classified into attractive and repulsive forces. The attractive forces are mainly van der Waals forces, electrostatic forces, chemical forces, etc. The repulsive forces are mainly electrostatic Coulombic interactions, capillary forces, covalent forces, etc. In general, the repulsive forces are very short-range forces and have an exponential decaying or show inverse power-law behavior which hugely depends upon the separation distance.

Van der Waals forces are the weakest forces which exist between the atoms and molecules and cumulatively hold atoms and molecules together. Their importance follows from two unique properties. Firstly, they are universal forces, which exist everywhere. All atoms and molecules attract one another through these interactions. They are responsible for cohesion of the inert gases in the solid and liquid states, and physical adsorption of molecules to solid surfaces, where no normal chemical bonds are formed. Secondly, the force is still significant when the molecules are comparatively far apart, and it is additive for large numbers of molecules. Van der Waals forces affect various properties of gases and also give rise to an attractive force between two solid objects separated by a small gap, which is important in adhesion and thus provides stability to colloids. To acquire the image resolution, AFMs can generally measure the vertical and lateral deflections of cantilever by using an optical lever as shown in Fig. 7.5.
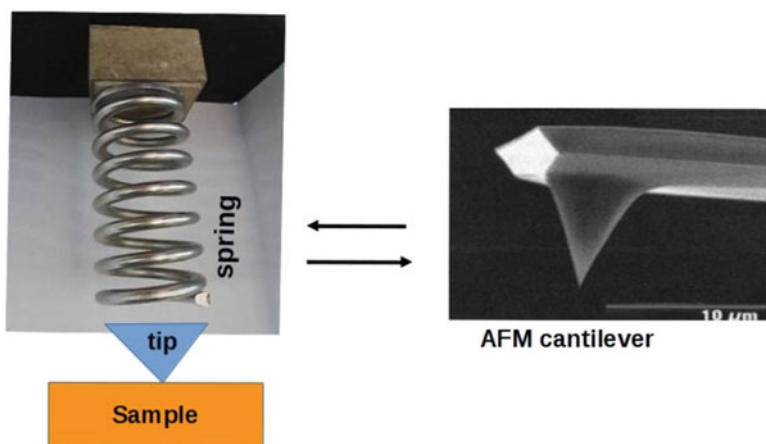

Fig. 7.4 AFM probe/tip attached to a flexible cantilever

Fig. 7.5 Schematic of the optical lever (adapted from [8]).

Photo detector

Laser

Laser beam

Piezo

Cantilever

Tip

Sample

Sample holder/ puck

Laser

Mirror

Photodiode

AFM Image

Cantilever

Sample

Piezo Scanner

z y x
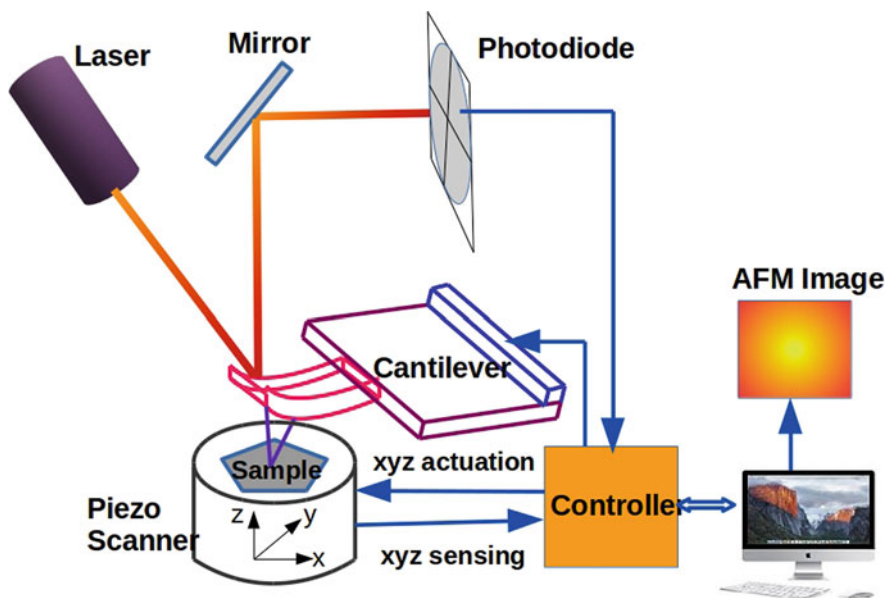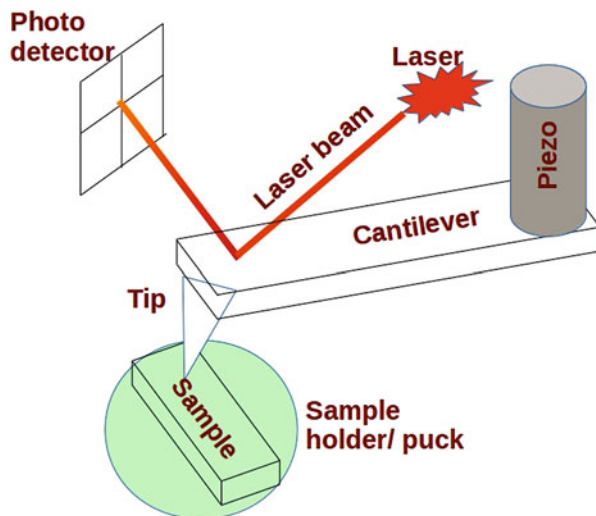
xyz actuation

xyz sensing

Controller

Fig. 7.6 Schematic of atomic force microscope (adapted from https://www.techbriefs.com/component/content/article/tb/supplements/pit/applications/27833).

The optical lever operates by reflecting a laser beam off the cantilever. The AFM consists of four major parts, a cantilever with a sharp tip, normally made of silicon or silicon nitride, mounted on a piezo scanner that drives the cantilever; a laser diode; and a position-sensitive detector, as shown in Fig. 7.6. As the tip scans over the sample's surface, the interactions between the AFM tip and the features on

the surface cause displacement of the cantilever. The reflected laser beam strikes a position-sensitive photodetector consisting of four segmented photodetector. The difference between the signals obtained from various segments of photodetector indicate the position of the laser spot onto the detector and, thereby the angular deflections of the cantilever (Fig. 7.5). When tip and specimen are brought close to each other, the force between them led to deflection of cantilever. The atomic force microscope creates topographic images of the surface by plotting the laser beam deflection as its tip scans over the surface. This design greatly improved the sensitivity of the design of the microscope as cantilever displacement can easily be amplified by the light path. Atomic resolution images of a variety of surfaces have been achieved with this design. However, the most important point of this design for biomedical purposes is that it makes operation of the atomic force microscope possible in ambient environments or in aqueous solutions at room temperature or at 37 °C. These conditions are required for imaging native biological samples in their functional and physiological environments.

By using AFM, one cannot only image the surface in atomic resolution but also measure the force at nanonewton (nN) scale. Therefore, one can obtain the force-distance curves and calculate the spring constant of the samples, various polymeric samples and biological membranes. AFM consists of a cantilever with a sharp tip/probe that is used to scan the specimen surface. The deflection of the cantilever is measured using a laser spot reflected from the top of the surface of cantilever into the photodiode. If tip is scanned at constant height, due to local curvature of the surfaces, the tip may collide with the sample surface causing damage to the tip or the samples. Hence, *feedback mechanism* is employed to adjust the tip-to-sample distance to maintain a constant force between the tip and the sample surface as shown in the schematic in Fig. 7.6. Traditionally, the sample is mounted on piezoelectric tube scanner that can move the sample in z direction for maintaining a constant force and the x and y direction to scan the sample. AFM can be operated in a number of modes depending on the application. The basic modes are the static mode and dynamic mode.

7.1.2.2   Different Working Modes of AFM

There are three primary imaging modes of operation in AFM [1, 3, 6, 7]:

  (i) Contact AFM: **<0.5 nm** probe-surface separation
 (ii) Intermittent contact (tapping mode AFM): **0.5–2 nm** probe-surface separation
(iii) Non-contact AFM: **0.1–10 nm** probe-surface separation

Contact Mode AFM

The static mode is performed in "contact" with the sample surface, where the overall force is repulsive in nature. The cantilever tip is dragged over the substrate main-

Fig. 7.7 Force versus
probe-sample separation
curve
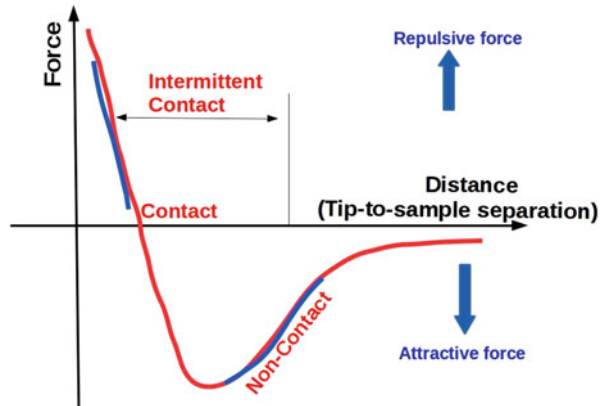
taining the deflection at a constant order. In contact mode, tip/probe experiences a
repulsive force with the sample surface. As the tip traces the sample, force on the
tip is repulsive; thus, cantilever bends away from sample to accommodate changes
in topography. To examine this force, we refer to force-distance curve in Fig. 7.7.

At larger distances, the atoms experience the attractive forces between them. As
the distance decreases, they weakly attract each other, on further approach of the
tip toward the sample; electron clouds begin to repel each other electrostatically,
and the atoms experience the repulsive forces. When the van der Waals force
becomes positive (repulsive), the atoms are in contact. Force between tip and
sample is determined by measuring the deflection of a spring cantilever. The force
is calculated by Hooke's law $F = -k\,X$, where "k" is the "spring constant" and
"X" is the displacement of the cantilever. The deflection of cantilever is used as
the input to feedback circuit that moves the scanner up and down in "z" direction.
The cantilever deflection constant (using the feedback loops) the force between the
probe and the sample remains constant and an image of the surface is obtained as
shown in schematic in Fig. 7.6.

The SPM controller is the heart of the instrument. It collects the signal and
converts it to height information using control electronics. The control system
performs two main functions:

(i) It generates drive voltage to control X-Y scans of the piezoelectric transducer.
(ii) It maintains incoming analog signal from microscope detection simultaneously
at a constant value through a feedback loop. The computer reads voltage from
comparator circuit through A/D converter. It is programmed to keep the two
inputs of the comparator circuit equal to 0 volts. An output voltage generated by
the computer continuously moves the piezoelectric transducer in the z direction
to correct for differences read into the A/D converter. This closed-loop feedback
control is the heart of the imaging portion of the control station.

Advantages: This mode provides fast scanning, and it is good for rough samples
and can be used in friction analysis.

Disadvantages: At times, forces can damage/deform soft samples.

Tapping (Intermittent) Mode AFM

In tapping mode, imaging is similar to contact; however, in this mode the cantilever is oscillated at its resonant frequency to avoid dragging the tip across the surface. The probe lightly "taps" on the sample surface during scanning, contacting the surface at the bottom of its swing (as in contact mode) and collects the data. Then go back at certain distance (as in non-contact mode). Cantilever amplitude is made constant in this mode. When tip passes over a bump surface, the amplitude oscillation decreases, and when tip passes over a depression, the amplitude increases. Amplitude oscillation is measured by the detection and used as input to controller electronics. The digital feedback loop then adjusts the tip separation to maintain constant amplitude and force on sample.

Advantages: Allows high resolution of samples that are easily damaged, good to use for biological samples
Disadvantages: More challenging to image in liquids, slower scan speeds needed

Non-contact Mode AFM

The non-contact mode is the dynamic mode since the cantilever is deliberately vibrated at or close to its resonance frequency. The resonance of the cantilever is characterized by amplitude, phase, and frequency. The variation of these three indicators, due to the interaction force, can be measured and generates an image. Obtaining atomic resolution in the dynamic mode is difficult in ambient conditions. In this mode, the probe does not contact the sample surface, but oscillates above the adsorbed fluid layer on the surface during scanning. Cantilevers used in this mode are stiffer than those used in contact mode. In non-contact AFM (NC-AFM), cantilever is oscillated slightly near its resonant frequency; change in frequency acts as input in feedback circuit to move scanner up and down. Feedback loop maintains constant frequency by maintaining tip-to-sample distance.

Advantages: As a very low force exerted on the sample (10–12 nN), the lifespan of the probe is increased.
Disadvantages: Generally gives lower resolution. The contaminant layer on surface can interfere with oscillation; therefore, it usually needs ultrahigh vacuum (UHV) to have the best imaging.

Limitations of AFM The AFM can be used to study a wide variety of samples (i.e., plastic, metals, glasses, semiconductors, and biological samples such as the walls of cells and bacteria). Unlike STM or scanning electron microscopy, it does not require a conductive sample. However there are limitations in achieving atomic resolution. The physical probe used in AFM imaging is not ideally sharp. As a consequence,

an AFM image does not reflect the true sample topography, but rather represents the interaction of the probe with the sample surface. This is called tip convolution.

7.1.2.3 Magnetic Force Microscopy (MFM)

Magnetic force microscopy (MFM) is a special mode of operation of the scanning probe microscope (SPM). The technique employs a magnetic probe, which is brought close to a sample and interacts with the magnetic stray fields near the surface. MFM was introduced shortly after the invention of the AFM (Martin and Wickramasinghe [12]) and became popular as a technique that offers high imaging resolution without the need for special sample preparation or environmental conditions. Since then, it has been extensively used in the fundamental research of magnetic materials, as well as the development of magnetic recording components.

7.1.2.4 Basic Working Principles of MFM

With the help of MFM, one can detect the magnetic domains within the sample. It is performed in lift mode, and it detects the phase change in the tip's oscillation due to magnetic strength of the domains lying in the sample. The operating principle of MFM is the same as in AFM, but it requires an additional lock-in amplifier to compare the phase and amplitude changes of the signal which arises due to sample's stray magnetic field as shown in Fig. 7.8.
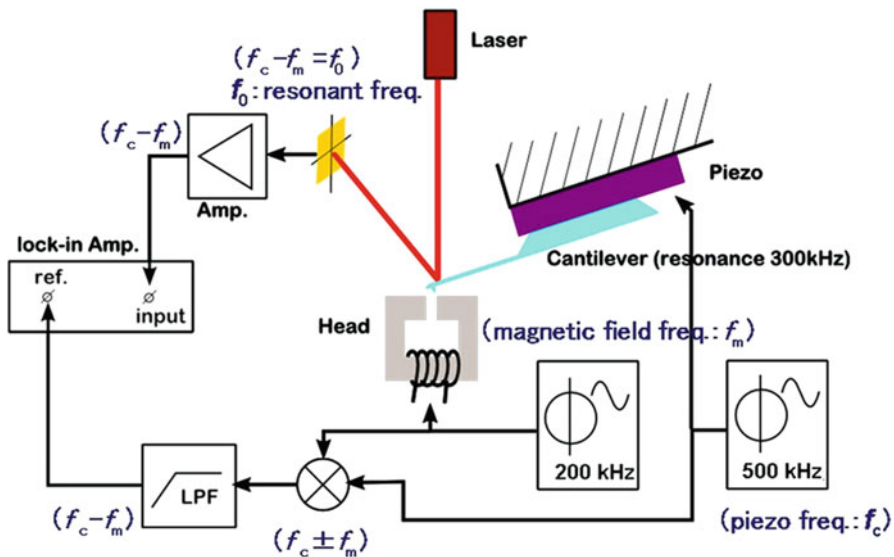

Fig. 7.8 Schematic of magnetic force microscopy setup (adapted from [13])

MFM images can be taken at different lift heights by lifting the tip at a certain distance above the sample in the lift mode. The scan is taken four times on the same line; magnetic interactions are taken during the second pass, where the topographic effect is subtracted from the MFM contrast. Both static and dynamic detection modes can be used for operation, but mainly the dynamic mode is considered as it can detect poor signals as well as, therefore, offers more sensitivity. More details are available in [13].

Here, the cantilever is oscillated by a piezoelectric element at an oscillation frequency, f_c, while the alternating magnetic field (driving frequency f_m) from the sample's stray field periodically modulates the effective spring constant of the cantilever. The frequency-modulated signals ($f = f_c - f_m$) are auto-selected by the mechanically oscillated tip. The driving voltages of the piezo and the sample are processed by a multiplier and low-pass filter. The processed signal is used as a reference for lock-in amplifier. The total signals due to magnetic field gradients, such as amplitude and phase, in-phase, and out-of-phase signals, can be detected simultaneously by the lock-in technique. The oscillation frequency (f_c) of the piezoelectric element is higher than the resonant frequency (f_0) of the tip. Therefore, one can get the information about the sample's magnetic strength by detecting the phase shift in the signals. The tip used in MFM mode is single-crystal Si coated with alloy of Co-Cr. The strength of the local magnetostatic interaction determines the vertical motion of the tip as it scans across the sample. The tip is magnetized every time before taking the measurements in the direction perpendicular to the plane of the film using a small permanent magnet to keep the directions of the spins same in the tip. Simultaneously, we obtained the topographic as well as magnetic images of the sample on the same spot locally. One can scan the samples at multiple points to get overall information about the sample's magnetic behavior [14–18].

7.1.2.5   Working Modes of MFM

The information about the sample's magnetic stray field can only be derived from MFM images when topographic signal contributions are not included. This is especially important when the tip is brought very close to the sample (in order to improve resolution), since nonmagnetic forces become increasingly stronger. The solution to this problem is to keep the topography influence constant by letting the tip follow the surface height profile [19]. This constant distance mode places higher demands on instrument stability, because it is sensitive to drift.

Therefore, one uses the specific method employed to separate signal contributions which is called lift mode (Fig. 7.9). It involves measuring the topography on each scan line in a first scan (left diagram), and the magnetic information in a second scan of the same line (right diagram).

The difference in height ∂h between the two scans is the lift height; it is selected by the user. Topography is measured in dynamic AM mode and the data is recorded to one image. This height data is also used to move the tip at a constant local distance above the surface during the second (magnetic) scan line, during which the feedback
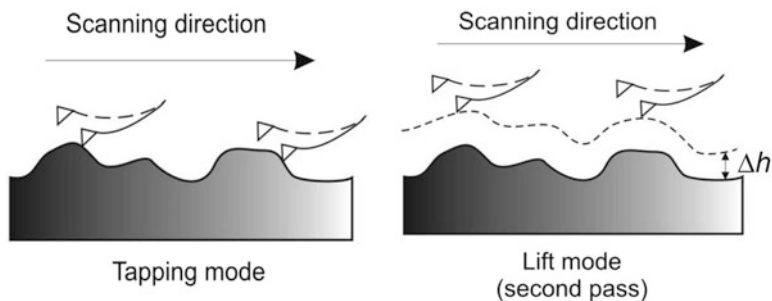
Fig. 7.9 Scanning the sample using lift mode in MFM. Magnetic information is recorded during the second pass in lift mode (adapted from [14])

is turned off. In theory, topographic contributions should be eliminated in the second image. Magnetic data can be recorded either as variations in amplitude, frequency, or phase of the cantilever oscillation. Therefore, MFM allows the imaging of relatively weak but long-range magnetic interactions. This measurement is unique as it gives us the idea about the localized magnetic domains within the magnetic films which no other technique can provide. All other techniques are used to detect magnetic strength of the films in bulk level or overall system. Especially, in the case of ion irradiation experiments, we get help to know how the ions have changed the magnetization locally as the ion beam is falling statistically onto the samples.

7.2   Applications

In the last few decades, extensive research has been done by our group to understand diversifying phenomena of the various materials using scanning probe microscopes in various modes such as STM, MFM, tapping AFM, IV spectroscopy in C-AFM, F-D curves using contact AFM, and many more [20–24]. In the next section, we are highlighting some of the important results.

7.2.1   AFM and MFM Studies on Co Nanoparticles

7.2.1.1   For Pristine Films

Thin films of Co with thickness ∼4 nm have been deposited on Si using thermal evaporation technique. The films were further irradiated with 120 MeV Ag ions at various ion fluences. Here, we are discussing only the example of the sample irradiated with a fluence of 1×10^{14} ions/cm^2. We have characterized the sample with Co-Cr-coated Si crystal tip in tapping mode. Upon scanning the pristine film of

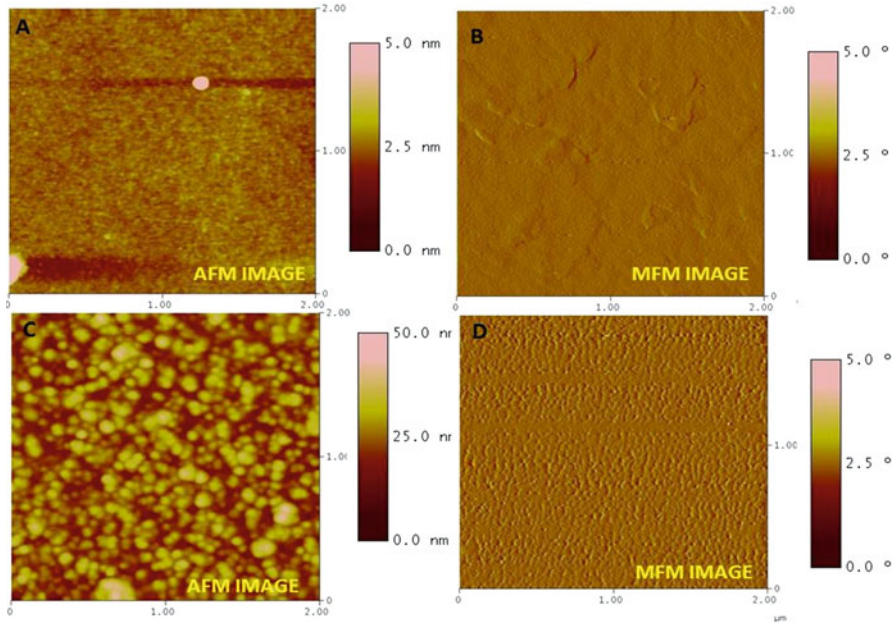**Fig. 7.10** AFM micrographs of pristine (**a**) and irradiated (**c**) thin-film (4 nm) samples of Co. MFM micrographs of pristine (**b**) and irradiated (**d**) thin-film (4 nm) samples of Co taken at a lift height of 50 nm

4 nm in MFM/lift mode, we could observe the smooth film with roughness 0.42 nm (given in Fig. 7.10a). Figure 7.10 is showing the AFM (a) and MFM (b) (topographic and the phase images, respectively) of the pristine sample at a lift height 50 nm.

In contrast to the AFM images, the MFM image shows good phase contrasts; the right side MFM/phase image shows the formation of domain/Bloch walls in the thin films, suggesting the magnetic nature of the cobalt is retained even after depositing in the form of a thinner layer of ∼4 nm. Although there is no magnetic cluster of particle formation, the overall film is magnetic in nature (Fig. 7.10b) with no preferred orientation or alignment. The domain walls can be seen with dark and bright contrast which is due to magnetic spin interaction of the sample and the tip. Bright reflects the alignment of the spins in the same direction (upward), and dark represents in opposite (downward). The intermediate or mean color contrast is due to the cancelation of spin up and down interaction between sample and the tip.

Apart from looking at the topography of the films, one can determine the size, height, and shape of the features too. Similarly we can find out the surface roughness of the films. Roughness is an important parameter for device applications and sensors. Figure 7.11 shows the sectional analysis of the pristine film with corresponding 3D view.

The AFM image shows a smoother film with smaller particle sizes ∼39 nm, as represented by red cursor (as shown in Fig. 7.11a, horizontal distance). The
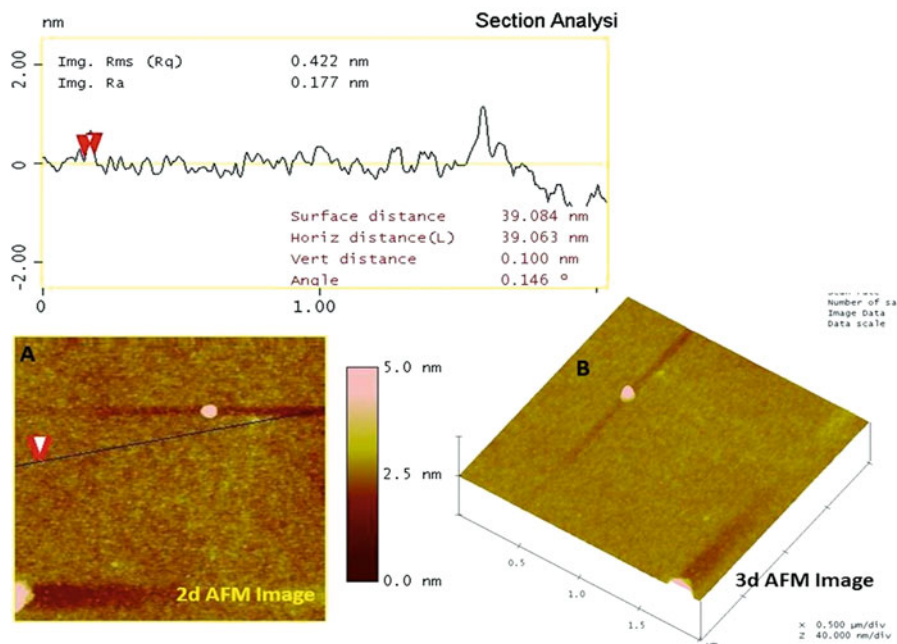
Fig. 7.11 (**a**) Section analysis of the pristine thin-film (∼4 nm) samples of Co and (**b**) 3D view of the pristine sample

corresponding rms value of the image was found to be ∼0.42 nm. Figure 7.11b represents a three-dimensional view of the pristine film to further confirm the formation of smoother films with not much height differences. Studies on Co thin-film samples after irradiation are given in the next section.

7.2.1.2 For Irradiated Films

The 4 nm thin-film sample of Co was irradiated with Ag 120 MeV swift heavy ions (SHI). The purpose of the irradiation was to form Co nanoparticles with uniform size distribution due to the impact of SHI with energy 120 MeV. The AFM and MFM images of the irradiated thin-film samples are shown in Fig. 7.10c, d, respectively. As can be observed, the irradiated films show granular morphology. However, this is only applicable for sample irradiated at 1×10^{14} ions/cm^2 in terms of uniformity of the structure sizes. The right panel (of Fig. 7.10d) shows that phase contrast is uniformly visible with no particular orientation. This is due to the fact that the irradiation dispersed Co grains with uniform magnetization on the surface.

Figure 7.12 shows the sectional analysis (a) of the irradiated film with corresponding 3D view (b). The AFM image shows a smoother film with smaller particle
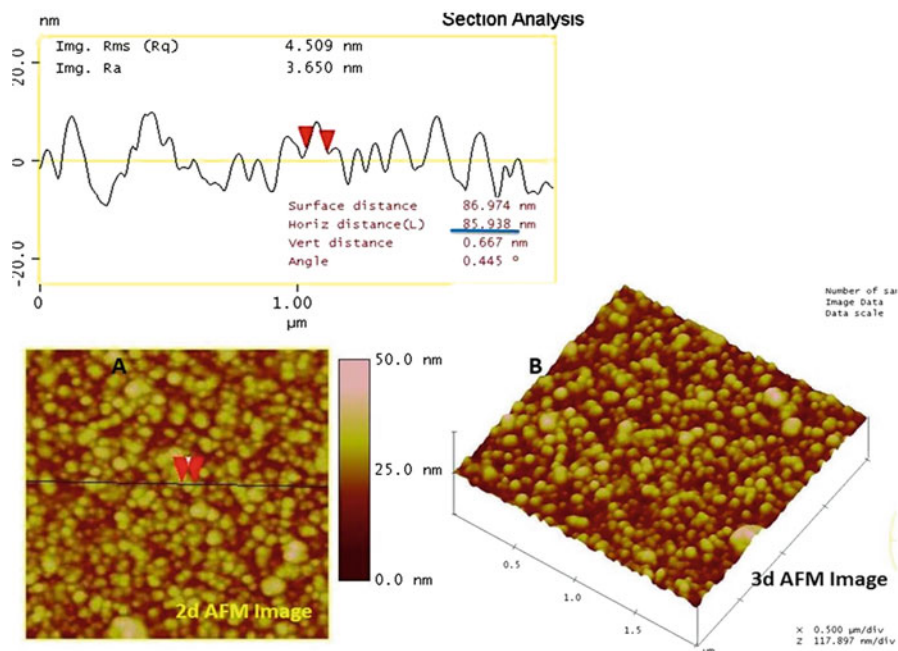
Fig. 7.12 (**a**) Section analysis of the irradiated thin-film (4 nm) samples of Co and (**b**) three-dimensional view of the irradiated sample

sizes ~85.9 nm, as represented by red cursor (as shown in Fig. 7.12a, horizontal distance).

The corresponding rms roughness value of the image was found to be ~3.7 nm. Figure 7.12b represents a 3D view of the irradiated film to further confirm the formation of uniform grains or nanoparticles with increased surface roughness. Further, in Fig. 7.11, we tried to find out the strength of magnetization in the pristine and irradiated thin-film samples through phase shift using section analysis. Figure 7.13a shows the phase shift due to magnetization as 0.53°, given by the peak-to-peak distance in vertical direction in the phase image captured in lift/MFM mode. The strength of magnetization has increased to 0.99° in the irradiated film as shown in Fig. 7.13b. This indicates that irradiation has resulted further into uniform Co nanoparticles formation; moreover, the magnetization has increased due to the effect of ion irradiation.

From the above study, one can say that due to irradiation the uniformly deposited thin film has resulted into well-ordered granular film of Co with an average size of ~90 nm. The magnetic strength of the film has increased upon irradiation. The granular film obtained after irradiation is uniform with uniform magnetization. In general, AFM and MFM provide a good morphological and phase contrast to the magnetic clusters.
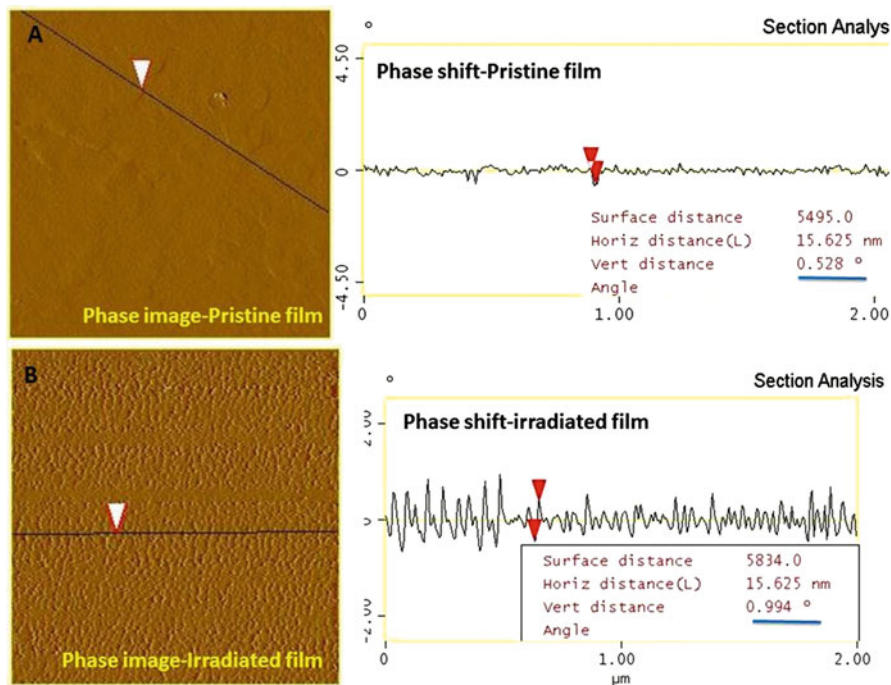
Fig. 7.13 Section analysis of MFM micrographs of pristine and irradiated Co 4 nm thin film

7.2.2 More Interesting Results Obtained from SPM in Various Modes

For more than a decade now, we have been using a multimode SPM with nanoscope IIIa controller acquired from Digital/Veeco Instruments Inc. (now Bruker, Singapore) installed at Inter University Accelerator Centre, New Delhi, in the following modes of operation in the user experiments: contact/tapping AFM, STM, MFM, and C-AFM. The areas of research include ion-induced surface morphology, SHI-induced modification in the size distribution, SHI-induced modification in magnetic domains, SHI-induced plastic flow of materials, and characterization of ion tracks in terms of size and number density. This system is actively being used by almost 70 institutes across India. Four of the illustrative images are taken in lift (tapping) mode MFM (Fig. 7.14), contact mode AFM (Fig. 7.15) tapping mode AFM (Fig. 7.16), and conducting mode (C-AFM) mode (Fig. 7.17). Tapping mode AFM for biological samples (Fig. 7.18) is given in the next section.
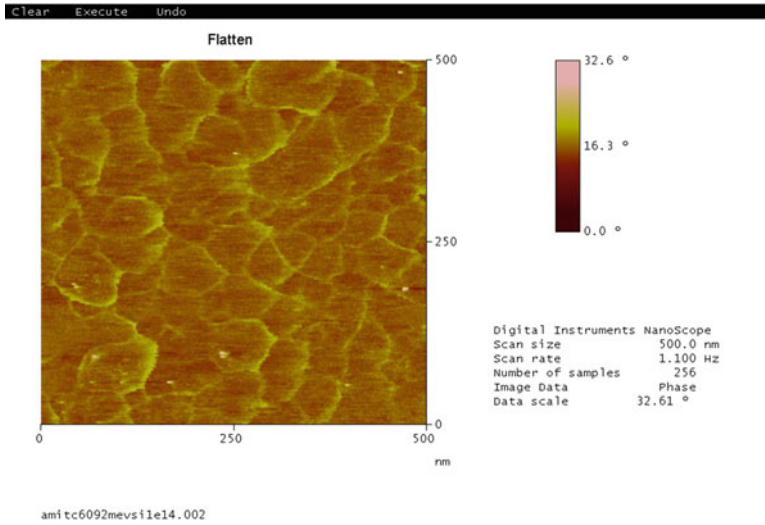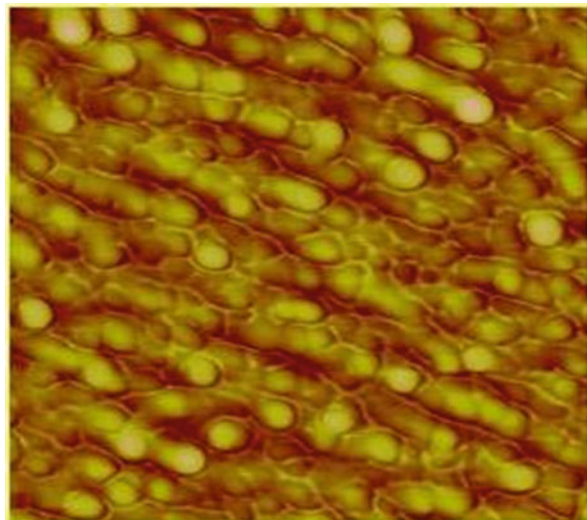
Fig. 7.14 Magnetic domains in fullerene films using MFM

Fig. 7.15 1.5 keV Ar
beam-induced ripple
formation on InP surface
using contact mode AFM

7.2.2.1 Magnetic Force Microscope

MFM image shows the phase contrast between the grain boundaries due to the influence of magnetic force (see Fig. 7.14). The image is taken at the lift mode where the van der Waals force (2–10 nm) diminishes and magnetic forces are active at a height (>10 nm). The sample was C-60 film and irradiated at 90 MeV Si ions at a fluence of 1×10^{14} ions/cm^2. Here, we would like to mention that the as-deposited film was not showing any magnetic signal. Due to irradiation some
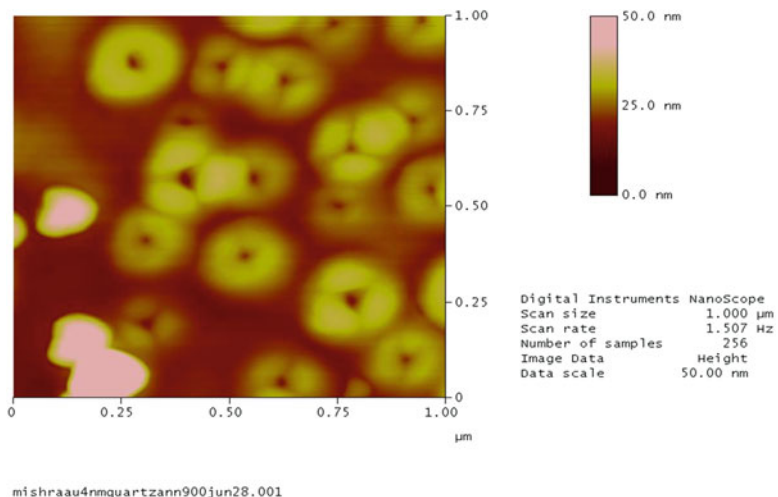
mishraau4nmquartzann900jun28.001

Fig. 7.16 Nanoring formations in Au thin films after annealing at 900 °C

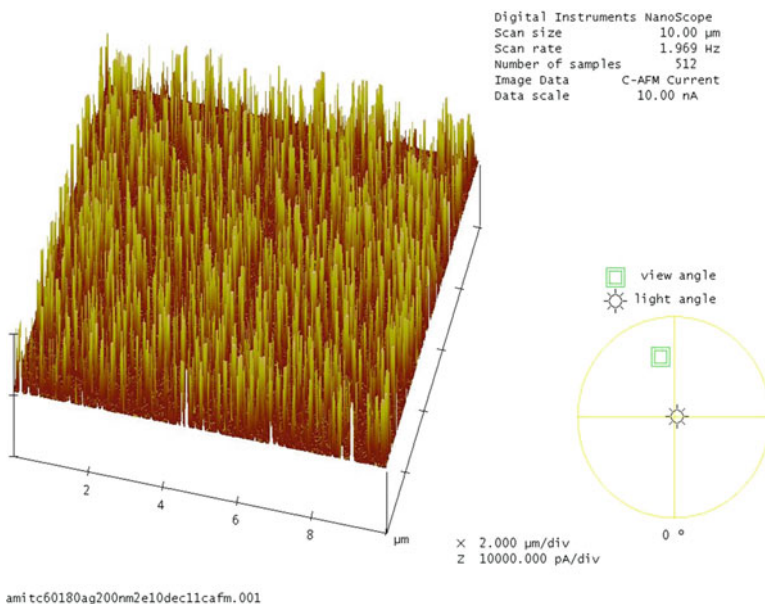amitc60180ag200nm2e10dec11cafm.001

Fig. 7.17 Conducting tracks in fullerene films by conducting AFM (C-AFM)

unpaired electrons have been generated at the grain boundaries and hence giving magnetic contrast. The track diameter was around 50 nm. This is a clear example of swift heavy ion (SHI)-induced magnetization of nonmagnetic film [17].

7.2.2.2 Contact Mode AFM

The AFM image performed in contact mode shows clearly the formation of ripple (Fig. 7.15). The sample was InP(100) substrate and bombarded with 1.5 keV Ar atoms. Due to high nuclear energy loss (S_n), it leads to displacement of atoms from their sites through collision cascades, and as the range of these atoms at this energy is about 40 nm so it will create modifications just below the surface and rippling is observed. The basics of ion-matter interaction can be read elsewhere. The main mechanism involved in such kind of pattern formation on the surface of any material is the interplay between the ion-induced sputtering or roughening and diffusion-induced smoothing of the surfaces.

Figure 7.16 is showing an example of nanoring formation in gold films, of thickness 4 nm deposited on quartz in UHV chamber at a base pressure of 10^{-8} Torr, obtained using the AFM image taken in tapping mode. The films were then annealed at 900 °C in Ar atmosphere. Interestingly, the films have shown the formation of nanorings. It was observed that at lower annealing temperatures, Au has agglomerated into clusters, whereas at 900 °C, three of such clusters have come together to form the ring (Fig. 7.16).

The above example shows that not only imaging but one can get the idea about how the agglomeration happen in certain kind of films (especially metallic films). These nanorings are formed to minimize the surface energies. Further annealing at higher temperatures may damage the ring formation.

7.2.2.3 Conducting Atomic Force Microscopy (C-AFM)

C-AFM image for C-60 film irradiated at 180 MeV Ag ions at 2×10^{10} ions/cm^2 showing the formation of ion tracks (see Fig. 7.17). Conducting ion tracks ($\sim$50 nm in diameter) were formed in the films due to the passage of the ions through it. In C-AFM, we apply the bias to the sample, and the conducting path is obtained as we increase the bias voltage.

The above figure is not he topography image but is the current image [17]. The three-dimensional view gives the idea about how much conducting the sample is in particular regions where the track formation has happened due to ion irradiation.

One can say that SPMs have been used on almost all kind of samples and in different modes to fulfill the user requirements as per need [20–24]. Conventional AFM can be routinely utilized to observe the topological features as well as to analyze the surface roughness to fabricate good device for reflectivity estimation, sensing, etc. On the other hand, MFM can be very useful to study the magnetic domains of the magnetic thin films. C-AFM is another important tool which helps to determine the local conductivity of the samples and is very important in the field of ion irradiation experiments as the ion falls statistically onto the samples and locally modifies the surface conductivity. Moreover there are fluid cells available as an attachment which helps us to study the live cell under AFM to determine the elasticity, etc. of the cell membrane.

7.2.2.4 Application in Imaging of Biological Samples

The atomic force microscope is an important tool to explore the area of imaging in biomolecules. Modifications and improvements to the atomic force microscope in the past two decades have enabled the observation of biological samples from large structures, such as hair and whole cells, down to individual molecules of nucleic acids and proteins with submolecular resolution as shown by Chang et al. [25] and Ushiki et al. [26]. The AFM image shown in Fig. 7.18 reveals the image of the human chromosomes.

The images of the chromosomes were obtained by AFM and SEM techniques and are compared here. The height of the specimens in the AFM image is displayed as color gradations. The AFM image corresponds well to the SEM image but has the advantage in giving height information of non-coated samples unlike as in scanning electron microscopy. Generally, AFM is considered to be a superior tool to explore these biomolecules as mostly they are in the order of few microns in length scales. Moreover, AFM has the unique ability to measure molecular forces with high sensitivity. These applications have been exploited to reveal structural details and define the molecular forces involved in a variety of biological systems.

Measurements of electrostatic characteristics are also among the emerging advances that can facilitate the analysis of biological and biomedical samples. The need for detailed imaging at the molecular level and for monitoring dynamic biological processes will continue. AFM is, therefore, likely to play an important and enduring role in biological and biomedical research. Nowadays, a large number of AFM applications in mammalian cell studies are related to cancer cells, while the mechanical properties of cancer cells have been measured by AFM and their use has been proposed for cancer cell identification.
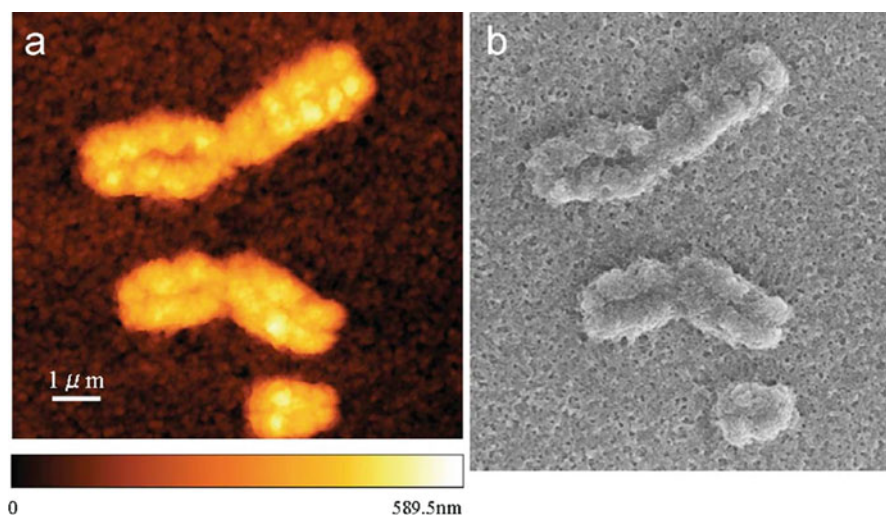

Fig. 7.18 (**a**) AFM and (**b**) SEM images of human metaphase chromosomes

7.3 Understanding the Surface Correlation for Co Nanoparticles

In this section, we will discuss how one can analyze the results obtained from AFM images using the correlation length, surface roughness, autocorrelation functions, and its importance to draw useful information for the samples using AFM images of Co thin-film samples.

Here, it is to be noted that the deposited thin films or ion-irradiated surfaces are not perfectly uniform. The surface height varies from point to point due to random elements in the growth process or after ion beam irradiation. Conventional statistical measures to characterize this height variation are measures of deviation like the mean deviation and the root mean square (rms) deviation. The mean deviation of the surface heights is called the average roughness, whereas the rms deviation is called the interface width. Interface width is the most important characteristic that describes the roughness of a surface.

However, interface width is not sufficient to describe the surface profile of a thin film because it does not provide any information about the observed correlation in surface heights. If the surface height is more than the average height at one point, it is very likely that the surface height in the neighborhood of the point is also more than the average height. Autocorrelation function, height-height correlation function, and lateral correlation length are used extensively to characterize these correlation properties. In recent times fluctuations in surface heights have been shown to exhibit self-affinity properties which are best characterized by techniques that have been developed for exploration of fractal objects. In this section, we introduce a set of useful statistical functions and techniques that have been used extensively in the literature to characterize the abovementioned properties of height fluctuations in thin film or ion-irradiated surfaces.

7.3.1 Surface Roughness

The root mean square value of the surface height, also known as interface width (w), and average roughness (R_a) of the surface are important parameters in quantitatively analyzing the characteristics of the surface morphology of thin films. Experimentally, the surface height is measured over a discrete lattice. From this discrete data, the interface width is computed as

$$w = \frac{1}{N} \sqrt{\sum_{i=1}^{N} \sum_{j=1}^{N} [h(i, j) - \langle h(i, j) \rangle]^2} \qquad (7.1)$$

whereas the average roughness R_a of the surface is computed as

$$R_a = \frac{1}{N^2} \sum_{i=1}^{N} \sum_{j=1}^{N} |h(i, j - \langle h(i, j) \rangle|$$ (7.2)

where $h(i,j)$ denotes height of the surface measured using the AFM at the point (i,j) and $\langle h(i,j) \rangle$ is their overall average over a total number of $N \times N$ points, which is given by

$$\langle h(i, j) \rangle = \frac{1}{N^2} \sum_{i=1}^{N} \sum_{j=1}^{N} h(i, j)$$ (7.3)

7.3.2 Correlation Functions

Average roughness and interface width characterize global roughness of a surface [27–29]. They do not characterize surface correlation, which is an important characteristic of the surface. Since correlation functions relate height fluctuations at different points, in defining correlation functions, it is very common to redefine the surface height profile such that $\langle h(i,j) \rangle = 0$ by choosing a suitable reference height. Unless otherwise stated, the mean height is taken to be zero at all times by replacing $h(i,j)$ with $(h(i,j) - \langle h(i,j) \rangle)$.

7.3.2.1 Autocorrelation Function

Autocorrelation function is very frequently used to characterize correlation properties. The one-dimensional autocorrelation function along the fast-scan direction x is usually evaluated from the height profiles $h(i,j)$ as

$$A(r = md) = \frac{1}{N(N-m)w^2} \sum_{j=1}^{N} \sum_{i=1}^{N-m} h(i+m, j) \; h(i, j)$$ (7.4)

where d is the horizontal distance between two adjacent pixels.

From Eqs. (7.1) and (7.3), it follows that $A(0) = 1$. Also we expect that the correlation decreases as r increases and becomes negligible for sufficiently large r. For thin-film surfaces, the autocorrelation function $A(r)$ is often found to have an exponentially decreasing behavior, and it approaches zero for large r. The value of r at which $A(r)$ decreases to $1/e$ is known as the lateral correlation length ξ. Thus,

$$A(\xi) \cong \frac{1}{e}$$ (7.5)

Therefore, the lateral correlation length ξ is defined as the length beyond which the surface heights are not significantly correlated.

7.3.2.2 Exponential Correlation Model

Several analytic expressions have been proposed for the autocorrelation function. A particularly simple form as

$$A(r) = \exp\left[-\left(\frac{r}{\xi}\right)^{2\alpha}\right] \tag{7.6}$$

where α is called the roughness exponent. The exponential correlation model (Eq. 7.6) does not work for $\alpha \to 0$ because the autocorrelation function becomes constant at $\alpha = 0$.

7.3.2.3 Height-Height Correlation Function

Another function used for characterizing correlation is the height-height correlation function H, which is calculated along the fast-scan direction x as

$$H(r) = \frac{1}{N(N-m)} \sum_{j=1}^{N} \sum_{i=1}^{N-m} [h(i+m, j) - h(i, j)]^2 \tag{7.7}$$

This function is especially useful for characterizing self-affine surfaces.

The relationship between the height-height correlation function and the autocorrelation function can be derived as follows:

$$
\begin{aligned}
H(r) &= \langle [h(i+m, j) - h(i, j)]^2 \rangle \\
&= \langle [h(i+m, j)]^2 \rangle + \langle [h(i, j)]^2 \rangle - 2\langle h(i+m, j)\, h(i, j) \rangle \\
&= w^2 + w^2 - 2\left(w^2 A(r)\right) \\
&= 2w^2 - 2w^2 A(r) \\
&= 2w^2 [1 - A(r)]
\end{aligned} \tag{7.8}
$$

Using Eq. (7.5), we have

$$H(\xi) = 2w^2(1 - 1/e) \tag{7.9}$$

In other words, we can say that the value of r at which $H(r)$ increases to $(1 - 1/e)$ is identified as the lateral correlation length ξ.

For surfaces which are self-affine on a short scale and for which the autocorrelation function vanishes for large separation, the height-height correlation function

$H(r)$ takes the scaling form

$$H(r) = \begin{cases} 2w^2, \text{ for } r >> \xi \\ r^{2\alpha}, \text{ for } r << \xi \end{cases} \tag{7.10}$$

For the exponential correlation model [30],

$$H(r) = 2w^2 \left[1 - \exp\left(\frac{r}{\xi}\right)^{2\alpha} \right] \tag{7.11}$$

This form is consistent with Eq. (7.10), because for $r < < \xi$,

$$H(r) \approx 2w^2 \left[1 - \left(1 - \left(\frac{r}{\xi}\right)^{2\alpha} \right) \right] \approx 2w^2 \frac{r^{2\alpha}}{\xi^{2\alpha}} \sim r^{2\alpha} \tag{7.12}$$

and for $r > > \xi$, it gives

$$H(r) \approx 2w^2 \tag{7.13}$$

For example, Fig. 7.10a, c shows AFM images of pristine and ion-irradiated thin films deposited for 4-nm-thick Co layer onto Si substrates by electron beam evaporation method at room temperature. The granules of various scales are present in the films, which have irregular shapes, different sizes, and separations. In quantitative analyses, the height roughness (R_a) and interface width (w) have been employed to describe the surface morphology. Here R_a is defined as the mean value of surface height relative to the center plane, and w is the root mean square (rms) value of the surface height. The roughness (R_a and w) is calculated using the method described in Sect. 5.2. The computed values for R_a and w are 0.7527 and 3.7341 nm and 1.0059 and 4.6570 nm corresponding to pristine and ion-irradiated surface, respectively. It is found that these values are increased with ion irradiation. The roughness parameters based on conventional theories depend on the sampling interval of measuring instrument. These parameters do not provide the complete outline like the shape of peaks and valleys of the thin-film surfaces. Average roughness (R_a) and interface width (w) are global measures of roughness but fail to describe the short-range variation of the surface roughness. These parameters are only sensitive to the peak values of surface profile. But, these parameters do not give information about irregularity/complexity of a surface.

The normalized autocorrelation function is computed to investigate the self-affine nature of thin-film surfaces applying the method described by Eq. (7.4). Figure 7.19 shows $A(r)$ versus r plot for pristine and ion-irradiated film. The $A(r)$ shows exponentially decreasing behavior of the surface which confirms that the surface under investigation has self-affine nature. The value of r at which $A(r)$ decreases to $1/e$ is known as the lateral correlation length ξ. We find that for pristine thin film, $A(r)$ do not decrease to $1/e$, while after irradiation it drops $1/e$ as depicted in Fig.
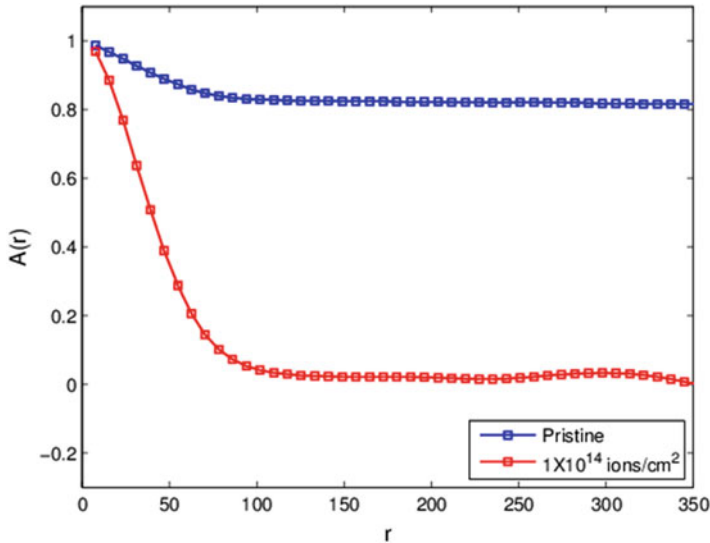
Fig. 7.19 Autocorrelation function for pristine and ion-irradiated 4 nm Co thin-film surfaces

7.19. The value of ξ for ion-irradiated Co thin-film surface is computed 48.6680 nm as shown in Fig. 7.20. It is found that the best-fit curve used to represent $A(r)$ for an isotropic self-affine surface may be written by Eq. (7.6). e provides vertical as well as lateral information about the surfaces. Here, ξ is the measure of length beyond the surface heights which are not significantly correlated.

The height-height correlation function $H(r)$ gives the same information as autocorrelation function $A(r)$. It is straightforward to show that the $H(r)$ and $A(r)$ are related by Eq. (7.8). The two clearly distinct regions are observed in $\log H(r)$ versus $\log r$, which marks the transition between power-law regime and the saturation regime. The turning point determines the value of ξ. Surface heights at points separated by a distance much larger than the lateral correlation length can be considered uncorrelated. Surface heights often exhibit self-affinity properties. The saturation value of $H(r)$, i.e., the value of $H(r)$ at which it forms a plateau, is very close to the value of $2w^2$ corresponding to that thin film as depicted in Fig. 7.21. The roughness exponent (α) is determined from a fit to the linear portion of the log-log plot of $H(r)$ versus r. The lateral correlation length ξ marks the transition between power-law region and the saturation region. Surface heights at points separated by a distance much larger than the lateral correlation length can be considered uncorrelated. Surface heights often exhibit self-affinity properties. For thin-film surfaces, self-affinity holds only for small r. Therefore, α characterizes only the short-range roughness of the surface. The roughness exponent α signifies the height fluctuation which corresponds to vertical growth of the thin film [31].
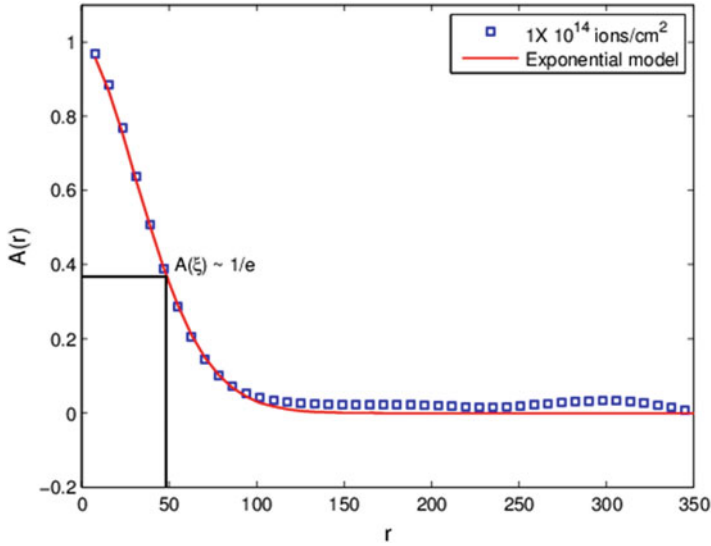
Fig. 7.20 Autocorrelation function A versus r
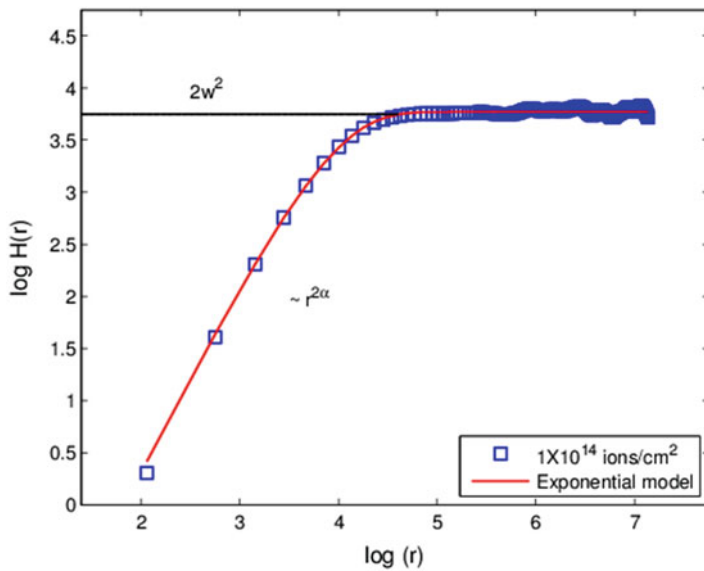

Fig. 7.21 Log H as a function of log r for each thickness. The solid lines are best-fit curves

7.4   Conclusion

It is concluded that the invention of AFM is indeed a boon to the researchers worldwide, to determine the surface topography of the variety of samples such as polymers, magnetic films, metals, glasses, semiconductors, and biological samples such as the walls of cells and bacteria, etc. It has become one of the most important tools for imaging the surfaces of samples at nanometric-scale resolution. Thus, it is considered to be a strong competitor to conventional methods, which are used to obtain the morphology of the samples and to investigate the structures, such as in electron microscopy, X-ray scattering, etc. Unlike STM or scanning electron microscopy, it does not require a conductive sample. However, limitations in achieving atomic resolution arise due to the use of physical probe which may not be ideally sharp. As a consequence, an AFM image does not reflect the true sample topography, but rather represents the interaction of the probe with the sample surface. Further, with MFM we came to know that the information about the sample's magnetic stray field can only be derived from MFM images when topographic signal contributions are not included. This is especially important when the tip is brought very close to the sample. Therefore, MFM allows the imaging of relatively weak but long-range magnetic interactions. This measurement is unique as it gives us the idea about the localized magnetic domains within the magnetic films which no other technique can provide. All other techniques are used to detect magnetic strength of the films in bulk level or overall system. Further, we understood that using the correlation lengths of the surface features, one can find out if the structures are self-affine or not. For thin-film surfaces, self-affinity holds only for small distances, r. Therefore, roughness exponent, α, characterizes only the short-range roughness of the surface; α signifies the height fluctuation which corresponds to vertical growth of the thin film.

References

1. Giessibl, F. J. (2003). Advances in atomic force microscopy. *Reviews of Modern Physics, 75*, 949.
2. Julian Chen, C. (2007). *Introduction to scanning tunneling microscopy* (2nd edn). Oxford University Press. Oxford Scholarship Online
3. Wiesendanger, R. (1994). *Scanning probe microscopy and spectroscopy: Methods and applications*. Cambridge, UK: Cambridge University Press.
4. *Scanning tunneling microscopy. Perspectives in condensed matter physics (a critical reprint series)* (Vol. 6). Dordrecht: Springer.
5. Binning G, ROhrer H. (1986) *Scanning Tunneling Microscopy, IBM Journal of Research and Development 30*(4), 355–369.
6. http://www.chembiouoguelph.ca/educmat/chm729/afm/detail.htm#tapping.
7. http://enwikipedia.org/wiki/Atomic-force-microscopy.
8. A. Yacoot and L. Koenders (2008), Aspects of scanning force microscope probes and their effects on dimensional measurement, J. Phys. D: Appl. Phys., 41, 103001.

9. https://www.techbriefs.com/component/content/article/tb/supplements/pit/applications/27833.

10. http://www.nanoscience.gatech.edu/zlwang/research/afm.html.

11. http://ipc.iisc.ernet.in/~ipcafm/about%20us.html.

12. New, R., Martin, Y., & Wickramasinghe H. K. (1987). Magnetic imaging by "force microscopy" with 1000 Angstrom resolution. *Applied Physics Letters, 50*, 1455(1987). https://doi.org/10.1063/1.97800 Y.

13. Zhenghua, L., Xiang, L., Dong, D., Dongping, L., Saito, H., & Ishio, S. (2014). AC driven magnetic domain quantification with 5 nm resolution *Scientific Reports, 4*, 5594.

14. Gomez, R. D., et al. (1998). Quantification of magnetic force microscopy images using combined electrostatic and magnetostatic imaging *Journal of Applied Physics, 83*, 6226.

15. Gomez, R. D., et al. (1996). Switching characteristics of submicron cobalt islands *Journal of Applied Physics, 80*(1), 342.

16. Landis, S., et al. (1999). Domain structure of magnetic layers deposited on patterned silicon *Applied Physics Letters, 75*, 2473.

17. Kumar, A., Avasthi, D. K., Pivin, J. C., Papaléo, R. M., Tripathi, A., Singh, F., & Sulania, I. (2007). Magnetic Force Microscopy of Nano-Size Magnetic Domain Ordering in Heavy Ion Irradiated Fullerene Films *Journal of Nanoscience and Nanotechnology, 7*(6), 2201.

18. Hartmann, U. (1999). MAGNETIC FORCE MICROSCOPY *Annual Review of Materials Research, 29*, 53–87.

19. Porthun, S., Abelmann, L., & Lodder, C. (1998). Magnetic force microscopy of thin film media for high density magnetic recording *Journal Magnetism Magnetic Materials, 182*, 238–273.

20. Sulania, I., Agarwal, D. C., Kumar, M., Kumar, S., & Kumar, P. (2016). Topography evolution of 500 keV Ar4+ ion beam irradiated InP(100) surfaces - formation of self-organized In-rich nano-dots and scaling laws *Physical Chemistry Chemical Physics, 18*(30), 20363–20370.

21. Sulania, I., Agarwal, D., Husain, M., & Avasthi, D. K. (2016). Investigations of ripple pattern formation on Germanium surfaces using 100-keV Ar+ ions *Nanoscale Research Letters, 10*(88), 1–8.

22. Sulania, I., Agarwal, D., Kumar, M., & Avasthi, M. (2013). Low energy bombardment induced formation of Ge nanoparticles *Advanced Materials Letters, 4*(6), 402.

23. Sulania, I., Tripathi, A., Kabiraj, D., Varma, S., & Avasthi, D. K. (2008). keV Ion-Induced Effective Surface Modifications on InP *Journal Nanoscience Nanotechnology, 8*(8), 4163–4167.

24. Mishra, Y. K., Kabiraj, D., Sulania, I., Pivin, J. C., & Avasthi, D. K. (2007). Synthesis and Characterization of Gold Nanorings *Journal Nanoscience Nanotechnology, 7*(6), 1878–1881.

25. Chang, K.-C., Chiang, Y.-W., Yang, C.-H., Liou, J.-W., & Chi, T. (2012). Atomic force microscopy in biology and biomedicine. *Medical Journal, 24*, 162–169.

26. Ushiki, T., & Hoshi, O. (2008). Atomic force microscopy for imaging human metaphase chromosomes. *Chromosome Research, 16*, 383–396.

27. Yadav, R. P., Kumar, T., Mittal, A. K., Dwivedi, S., & Kanjilal, D. (2015). Fractal characterization of the silicon surfaces produced by ion beam irradiation of varying fluences *Applied Surface Science, 347*, 706–712.

28. Yadav, R. P., Dwivedi, S., Mittal, A. K., Kumar, M., & Pandey, A. C. (2012). Fractal and multifractal analysis of LiF thin film surface *Applied Surface Science, 261*, 547–553.

29. Yadav, R. P., Kumar, M., Mittal, A. K., & Pandey, A. C. (2015). Fractal and multifractal characteristics of swift heavy ion induced self-affine nanostructured BaF2 thin film surfaces *Chaos, 25*, 083115.

30. Pelliccione, M., & Lu, T. M. (2008). *Evolution of thin film morphology: Modeling and simulations*. Berlin: Springer.

31. Yadav, R. P., Kumar, M., Mittal, A. K., Dwivedi, S., & Pandey, A. C. (2014). On the scaling law analysis of nanodimensional LiF thin film surfaces *Materials Letters, 126*, 123–125.